EUROFUSION WPMST1-PR(16) 16622

WA Suttrop et al.

Role of plasma shape and rotation for access to suppression of edge-localized modes by magnetic perturbations in a shape-matching identity experiment in ASDEX Upgrade and DIII-D

Preprint of Paper to be submitted for publication in
Physical Review Letters

This work has been carried out within the framework of the EUROfusion Consortium and has received funding from the Euratom research and training programme 2014-2018 under grant agreement No 633053. The views and opinions expressed herein do not necessarily reflect those of the European Commission.

This document is intended for publication in the open literature. It is made available on the clear understanding that it may not be further circulated and extracts or references may not be published prior to publication of the original when applicable, or without the consent of the Publications Officer, EUROfusion Programme Management Unit, Culham Science Centre, Abingdon, Oxon, OX14 3DB, UK or e-mail Publications.Officer@euro-fusion.org

Enquiries about Copyright and reproduction should be addressed to the Publications Officer, EUROfusion Programme Management Unit, Culham Science Centre, Abingdon, Oxon, OX14 3DB, UK or e-mail Publications.Officer@euro-fusion.org

The contents of this preprint and all other EUROfusion Preprints, Reports and Conference Papers are available to view online free at http://www.euro-fusionscipub.org. This site has full search facilities and e-mail alert options. In the JET specific papers the diagrams contained within the PDFs on this site are hyperlinked

Role of plasma shape and rotation for access to suppression of edge-localized modes by magnetic perturbations in a shape-matching identity experiment in ASDEX Upgrade and DIII-D

W. Suttrop,[1,*] R. Nazikian,[2] A. Kirk,[3] V. Bobkov,[1] M. Cavedon,[1] M. Dunne,[1] T. E. Evans,[4] B. A. Grierson,[2] A. W. Hyatt,[4] Y. Q. Liu,[3] B. Lyons,[4] R. M. McDermott,[1] H. Meyer,[3] T. Odstrčil,[1] D. Orlov,[5] T. H. Osborne,[4] C. Paz-Soldan,[4] D. A. Ryan,[3] E. Viezzer,[1,6] M. Willensdorfer,[1] ASDEX Upgrade, MST1,[†] and DIII-D Teams

[1]*Max-Planck-Institut für Plasmaphysik, D-85740 Garching, Germany*
[2]*Princeton Plasma Physics Laboratory, PO Box 451, Princeton, New Jersey 08543-0451, USA*
[3]*CCFE Culham Science Centre, Abingdon, Oxon, OX14 3DB, UK*
[4]*General Atomics, PO Box 85608, San Diego, California 92186-5608, USA*
[5]*UC San Diego, 9500 Gilman Drive, La Jolla, CA 92093, USA*
[6]*University of Seville, Seville, Spain*

(Dated: November 8, 2016)

In a plasma shape matching identity experiment in the DIII-D and ASDEX Upgrade, complete suppression of edge-localized modes (ELMs) by magnetic perturbations (MP) is obtained in both tokamaks in high-confinement mode (H-mode) with similarly good performance (H-mode confinement factor $H98P_{y,2} = 0.95$) at ITER-relevant pedestal collisionalities ($\nu^*_{\rm ped} = 0.1 - 0.3$). This scenario is compatible with the all-metal wall of ASDEX Upgrade. Fast decay of intentionally injected tungsten impurities indicates efficient outward transport of heavy impurities despite the absence of ELMs, supporting the applicability of ELM suppression for ITER. In DIII-D, the ELM suppression operating range is extended towards the matching shape at reduced triangularity ($\delta = 0.32$). In ASDEX Upgrade, this moderate degree of shaping leads to increased pedestal pressure and confinement compared to plasmas with even lower triangularity and was found essential to reproduce ELM suppression. Considerable variation of the ion and electron flow is encountered in these plasmas, including cases with finite cross-field electron fluid flow in the entire ASDEX Upgrade plasma. This finding suggests that access to ELM suppression may be possible in ITER at low torque input even if two-fluid models predict strong shielding of the resonant MP.

PACS numbers: 28.52.s, 52.55.Fa, 52.55.Rk

The transient heat load onto the first wall associated with edge-localized modes (ELMs) is a main concern for the ITER next step fusion device [1] and for a fusion reactor. Complete ELM suppression by small magnetic perturbations (MP) to the axisymmetric tokamak, first demonstrated in DIII-D [2], is the chief method considered for ITER. ELM suppression has been reproduced recently in KSTAR [3] and EAST [4], albeit at higher edge pedestal collisionality than in DIII-D and ITER. ASDEX Upgrade (AUG) has a magnetic perturbation coil set very similar to that of DIII-D [5]. With $n = 1, 2$ and 4 magnetic perturbations, reliable ELM mitigation is obtained [6]. Attempts to obtain ELM suppression in AUG had previously been unsuccessful despite similar plasma size of AUG and DIII-D and matching pedestal collisionality ($\nu^*_{\rm ped} = 0.1 - 0.3$). This difficulty raised concerns that a hidden parameter may be controlling access to ELM suppression, with plasma shape and effects of the different wall materials in DIII-D and ASDEX Upgrade being obvious candidates. Here, we report on a similarity experiment to resolve this question. In a first step, a plasma shape scan was performed in DIII-D, starting with ELM suppression by magnetic perturbations with $n = 3$ in a well established ITER similar shape (ISS) [7], then reducing upper and lower triangularity towards a plasma shape that was then matched in AUG in a second step. This approach proved successful in that with the matching shape, ELM suppression was indeed obtained in AUG, for the first time. Moreover, this is the first demonstration of ELM suppression with an all-metal wall (in AUG), an important aspect in view of its applicability in ITER which will have a metal wall as well.

Fig. 1 compares the DIII-D ISS (black) and matching shapes in DIII-D (red) and AUG (blue). The AUG cross section is enlarged by a factor of 1.19 which reflects a mismatch of aspect ratio that cannot be avoided in this experiment. Upper and lower triangularity of the matching shape are $\delta_u = 0.2$ and $\delta_l = 0.44$, respectively, whereas for the ISS, $\delta_u = 0.34$ and $\delta_l = 0.65$. During the DIII-D shape scan care was taken to maintain ELM suppression by adjusting the edge safety factor q_{95} and I-coil current. Two windows for ELM suppression at $q_{95} = 3.7$ and $q_{95} = 3.4$ were used and found to be unchanged as the plasma shape was varied.

Fig. 2 shows time traces of two shots at the extreme ends of the shape scan, pulse 164278 in ISS (black) and pulse 164362 (red) in the AUG-matching shape at the same edge electron pedestal collisionality, $\nu^*_{\rm ped} = 0.3$. Application of similar $n = 3$ resonant vacuum field results in marginal access to ELM suppression in both shots, as indicated by the recurrence of type-I ELMs during the MP phases. The H-mode confinement factor $H98P_{y,2}$ [8] in ELM suppressed phases ranges between $H98P_{y,2} = 0.95$ (164362, matching shape) and $H98P_{y,2} = 1.2$ (164278, ISS).

* Corresponding author e-mail address: Wolfgang.Suttrop@ipp.mpg.de

† See the author list of "Overview of progress in European Medium Sized Tokamaks towards an integrated plasma-edge/wall solution" by H. Meyer et al, to be published in Nuclear Fusion Special issue: Overview and Summary Reports from the 26th Fusion Energy Conference (Kyoto, Japan, 17-22 October 2016)

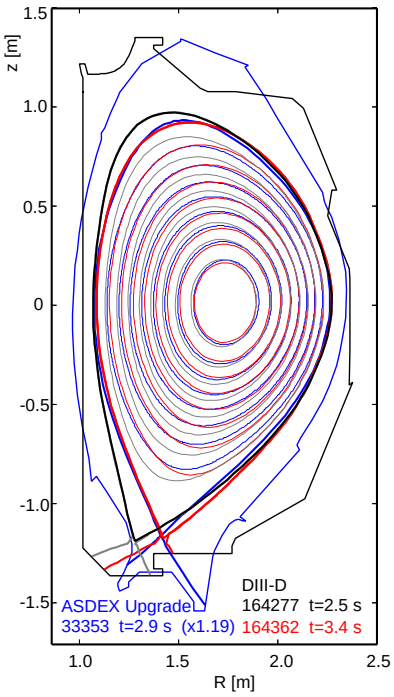

FIG. 1. Poloidal cross sections of the ITER-similar shape in DIII-D (black) and matching plasma shapes in DIII-D (red) and ASDEX Upgrade (blue, scaled by a factor of 1.19).

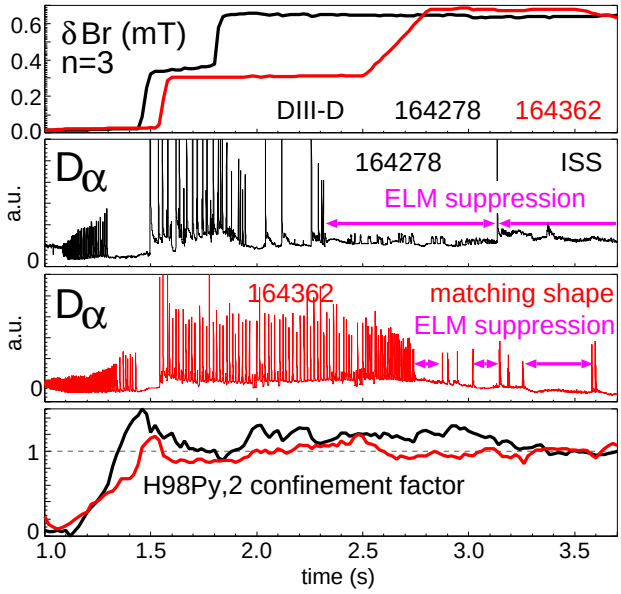

FIG. 2. Time traces of DIII-D discharge 164278 with ITER-similar shape and discharge 164362 with AUG-matching shape, showing similar performance and both marginal access to ELM suppression with similar $n = 3$ perturbation field strength.

Reproducible ELM suppression is obtained in AUG in plasmas with the matching shape, while for lower triangularity and otherwise similar plasma parameters ELMs persist, albeit with much reduced energy loss [9]. Fig. 3 shows time traces of discharge 33595 (matching shape) with a long stationary phase of ELM suppression which, once established at $t = 3.0$ s, lasts for the entire flat top duration. An $n = 2$ magnetic perturbation with differential phase $\Delta\Phi = 90^\circ$ (as defined in Refs. [6, 10]) between upper and lower coils is applied early after H-mode is reached. This phasing corresponds to best coupling to edge kink-peeling modes for these plasmas in analogy to the plasma configurations studied in Refs. [10, 11]. The H-mode phase shows frequent small ELMs at the beginning, which are suddenly suppressed as the pedestal electron density drops to 2×10^{19} m^{-3}, corresponding to a pedestal electron collisionality of $\nu^*_{ped} = 0.3$, after the gas puff has been reduced to a very low rate, 1×10^{21} D/s. The H-mode confinement factor $H98P_{y,2}$ [8] in the initial ELMy phase is $H98P_{y,2} = 1.0$ and drops to $H98P_{y,2} = 0.9 - 0.95$ at later times during the suppressed phase. Full suppression of ELMs is indicated by a large number of signals, e.g. the outer divertor thermoelectric current which is a reliable indicator of divertor temperature and therefore, ELM-related heat pulses. In the suppression phase, transient heat pulses from sawtooth crashes are observed; however the magnetic measurements indicate that in most cases they do not trigger ELMs.

A special feature of AUG is its fully tungsten-clad first wall, in contrast to graphite and carbon-fiber composites used as first wall materials in DIII-D. Stable H-mode operation with a metal wall requires net outward transport of heavy impurities to avoid radiative collapse of the plasma core [12], which is normally assisted by gas puffing in order to avoid density profile peaking and to ensure a sufficiently large ELM frequency. In AUG, the ITER-like low pedestal collisionality required for ELM suppression can only be achieved without strong gas puff. Therefore, it is important to verify that impurity accumulation can be avoided in the absence of ELMs. Two pulses of tungsten impurities are injected into discharge 33595 (bottom panel of Fig. 3) which are produced by using a monopole phasing instead of optimum power distribution between the straps of the newly installed 3-strap ICRF antenna [13]. The resulting tungsten influx from the outer limiter can be seen as an increased intensity of WI (neutral tungsten) spectroscopic lines. A small increase of tungsten concentration (higher charge states measured by an X-ray spectrometer) and main chamber radiated power follows and recovers to a steady state after about 200 ms, with a time constant slightly above the energy confinement time, $\tau_W \approx 1.2\tau_E$. Hence, a particle transport mechanism is active which is not only causing the "pump-out" of main ions but also flushes heavy impurities. This is consistent with the observation of outward transport of medium-Z impurities (flourine) in DIII-D [14].

Profiles of electron and ion temperature, electron density and total kinetic pressure in the edge pedestal region taken during ELM suppression are shown in Fig. 4 for DIII-D pulses 164277 (ISS) and 164362 (matching shape) as well as AUG pulses 31128 (ELM mitigation, low triangularity) and 33353 (ELM suppression, matching shape). While electron density and temperature are similar in the matching shape pulses in DIII-D and AUG, the impurity ion temperature profiles differ significantly between the machines by approximately a factor

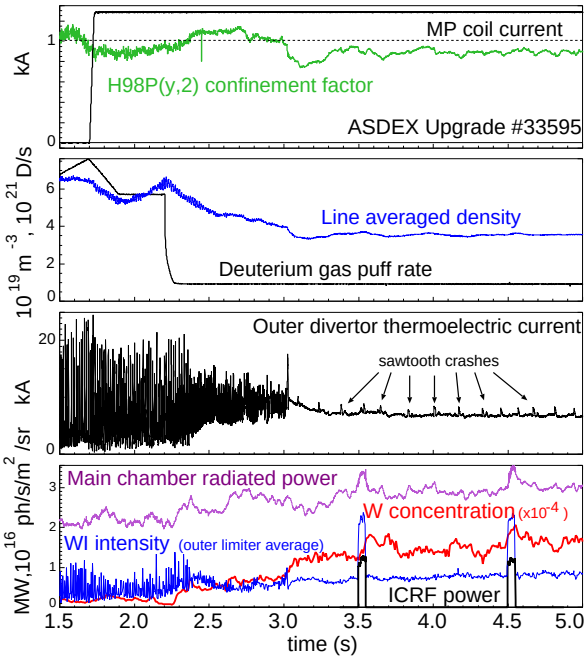

FIG. 3. Time traces of ASDEX Upgrade discharge 33595 showing ELM suppression after $t = 3.0$ s. ICRF pulses at $t = 3.5$ s and $t = 4.5$ s in monopole phasing provoke increased tungsten influx from the outer limiters – the plasma tungsten concentration recovers quickly.

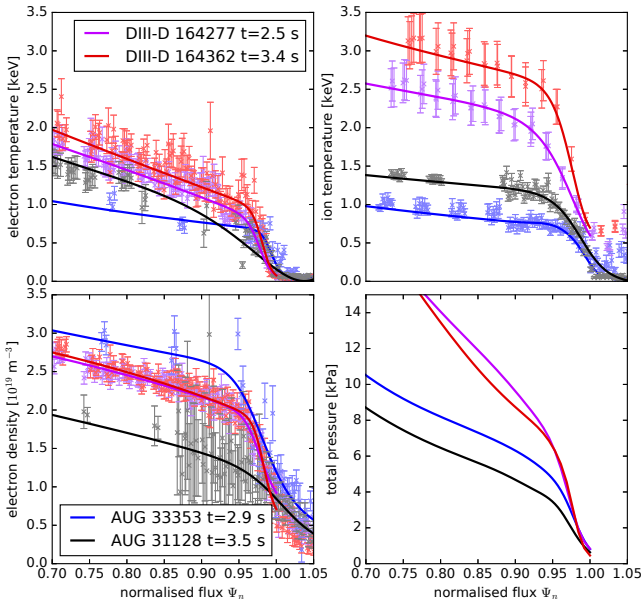

FIG. 4. Comparison of edge electron temperature (top left), ion temperature (top right), electron density (bottom left) and total pressure (bottom right) during ELM suppression for ASDEX Upgrade (AUG) pulses 31128 (low δ, black) 33353 (matching shape, blue) and DIII-D pulses 164277 (ISS, purple), 164362 (AUG matching shape, red).

of 2.5, not only at the plasma edge as shown but over the entire radius. The total kinetic pressure however, is less different and in fact is well matched in the plasma center. DIII-D shot 164362 has unusually high $Z_{\rm eff} \approx 4.5$ originating from carbon impurities. This is typically seen in matching shape plasmas for which the outer strike point has to be placed on top of the pump shelf instead of a good pumping position near the slit entrance (see Fig. 1). Apparently, the high ion temperature is compensating for the ion dilution in these DIII-D plasmas.

A recent model for ELM suppression [15] invokes an unshielded resonant response to the MP to block the expansion of the edge transport barrier before an ELM crash can occur. An essential aspect of this model, vanishing cross-field electron flow at resonant surfaces near the inner barrier edge, can be examined in our new experiment, based on charge exchange measurements on carbon (C^{6+}) in DIII and boron (B^{5+}) in AUG and using the impurity and electron radial force balance. Fig. 5 shows for DIII-D pulses 164277 (ISS) and 164362 (matching shape, left) and two AUG pulses (33353 and 33133, right), the measured and fitted impurity density (top panels) and impurity toroidal rotation frequency $\omega_{\rm tor}^{C6+}$ and $\omega_{\rm tor}^{B5+}$, respectively (bottom panels, solid lines). In the two AUG shots $\omega_{\rm tor}^{B5+}$ differs significantly, where in shot 33133 it is much smaller than in all other cases. The radial electric field is obtained from the impurity radial force balance [16], using the measured impurity temperature and density to calculate the impurity diamagnetic frequency $\omega^*_{\rm imp}$. The poloidal impurity rotation $\omega_{\rm pol}$ is not measured in these two AUG pulses, but calculated using the NEOART code [17, 18], while in DIII-D the poloidal rotation is taken from the charge exchange measurement. In AUG, the resulting $E \times B$ rotation frequency (dashed lines in Fig. 5, bottom right panel) in the plasma core and on the pedestal top ($\psi_N < 0.9$) is mainly determined by the toroidal flow, since the contributions of $\omega^*_{\rm imp}$ and $\omega_{\rm pol}$ to the force balance are very small there. With co-injected neutral beams as used in all present discharges, we have $\omega_{E\times B} > 0$ (ion diamagnetic direction) in the core. In the steep gradient region ($\psi_N > 0.93$), both poloidal and diamagnetic flows contribute to $\omega_{E\times B}$, which is negative there (inward directed radial electric field). Consequently, $\omega_{E\times B} = 0$ at a surface near the pedestal top and despite strong core rotation variations the radius of this surface varies little, $\psi_N \approx 0.95 - 0.96$ for the DIII-D shots and $\psi_N \approx 0.87$ and $\psi_N \approx 0.93$ for AUG shots 33133 and 33353, respectively. The perpendicular electron frequency $\omega_{e,\perp}$ (dotted lines in Fig. 5) is calculated from the electron radial force balance, which uses $\omega_{E\times B}$ and the electron diamagnetic frequency $\omega^*_{\rm e}$ as calculated from profile fits like those shown in Fig. 4. Given the impurity ion charge, $Z_{\rm imp} = 5$ (boron) or $Z_{\rm imp} = 6$ (carbon), $|\omega^*_{\rm e}| \approx Z_{\rm imp}|\omega^*_{\rm imp}|$ and therefore $\omega_{e,\perp}$ is always significantly offset from $\omega_{E\times B}$. In DIII-D shot 164362 at $t = 3.4$ s (during ELM suppression) $\omega_{e,\perp} = 0$ at $\Psi_N \approx 0.88$, at a clear distance from the $q = 10/3$ surface at $\Psi_N = 0.925$, which is bounding the edge gradient region. For AUG shot 33133 our analysis suggests that $\omega_{e,\perp} < 0$ in the entire pedestal region without crossing zero. In two-fluid MHD models [19–21], $\omega_{e,\perp} = 0$ is a necessary condition to avoid shielding of the external MP at rational surfaces and thus in the model of Ref. [15] this condition must hold at the pedestal top to explain ELM suppression [15]. In shot 33133 at the $q = 6/2$ surface ($\psi_N = 0.89$, on the

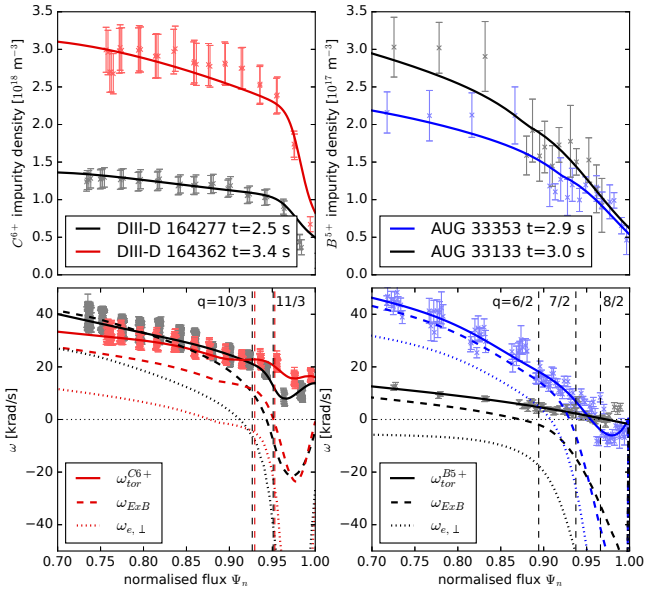

FIG. 5. Comparison of DIII-D shot 164362 (left, early and late time) and AUG shots 33353 and 33133 (right) during ELM suppression. Top: impurity density from charge exchange spectroscopy (C^{6+} and B^{5+}, respectively). Bottom: frequencies of toroidal impurity rotation (solid), $E_r \times B$ rotation (dashed) and cross-field electron flow (dotted).

pedestal top), $\omega_{e,\perp} = -20$ krad/s, which corresponds to significant shielding. If a resonant response is important for ELM suppression at all then these experimental cases cannot be explained by a fluid description. Kinetic modeling [22] suggests the role of a guiding center resonance at $\omega_{E\times B} = 0$ for field penetration and particle transport. In our present experiment, a surface with $\omega_{E\times B} = 0$ exists because of co-current $E \times B$ rotation in the core and it is always aligned with the inner boundary of the H-mode barrier. The sensitivity of ELM suppression to the $\omega_{E\times B} = 0$ location will be tested in future experiments.

In conclusion, our DIII-D/AUG similarity experiment demonstrates that at least moderate plasma shaping is essential to obtain ELM suppression. This finding explains why only ELM mitigation has been observed before in AUG despite otherwise similar plasma parameters [6]. Moderate shaping leads to increased edge pressure and can thereby potentially cause increased ideal kink plasma response. This picture is strengthened by the observation of similar pedestal pressure (Fig. 4) in the DIII-D ISS and matching shapes suggesting a similar plasma response. More detailed response modeling is underway to address this question.

The experiment also shows that ELM suppression can be robustly achieved with a metal wall, with stationary impurity density during extended ELM suppressed phases and outward transport of transiently injected impurities. This is a reassuring result in view of ITER which will also have a metal wall. In AUG, the required low pedestal collisionality precludes the use of gas puffing to produce flat density profiles which are favorable to avoid tungsten accumulation. In ITER, the same value of ν^* corresponds to larger plasma density than in AUG and in all likelihood significant fueling will be necessary which adds actuators and therefore additional degrees of freedom to tailor the density profile shape.

ACKNOWLEDGMENTS

This work was supported by the US Department of Energy contract DE-AC02-09CH11466. It has also been carried out within the framework of the EUROfusion Consortium and has received funding from the Euratom research and training programme 2014-2018 under grant agreement No 633053. The views and opinions expressed herein do not necessarily reflect those of the European Commission.

[1] A. Loarte *et al.*, Nuclear Fusion **54**, 033007 (2014).
[2] T. E. Evans *et al.*, Phys. Rev. Lett. **92**, 235003 (2004).
[3] Y. M. Jeon *et al.* (KSTAR team), Phys. Rev. Lett. **109**, 035004 (2012).
[4] Y. Sun *et al.*, Phys. Rev. Lett. **117**, 115001 (2016).
[5] W. Suttrop *et al.*, Fusion Engineering and Design **84**, 290 (2009).
[6] A. Kirk *et al.*, Nuclear Fusion **55**, 043011 (2015).
[7] T. E. Evans, M. E. Fenstermacher, R. A. Moyer, T. H. Osborne, and J. G. Watkins, Nuclear Fusion **48**, 024002 (2008).
[8] ITER Physics Expert Group on Confinement and Transport, ITER Physics Expert Group on Confinement Modelling and Database, and ITER Physics Basis Editors, Nuclear Fusion **39**, 2175 (1999).
[9] W. Suttrop *et al.*, "Experimental studies of high-confinement mode plasma response to non-axisymmetric magnetic perturbations in asdex upgrade," Accepted for publication in Plasma Phys. Control. Fus.
[10] M. Willensdorfer *et al.*, Plasma Physics and Controlled Fusion **58**, 114004 (2016).
[11] Y. Liu *et al.*, Nuclear Fusion **56**, 056015 (2016).
[12] R. Neu, IEEE Transactions on Plasma Science **38**, 453 (2010).
[13] V. Bobkov *et al.*, "First results with 3-strap ICRF antennas in ASDEX Upgrade," (2016), submitted to Nucl. Fus.
[14] B. A. Grierson *et al.*, Physics of Plasmas **22**, 055901 (2015), http://dx.doi.org/10.1063/1.4918359.
[15] M. Wade *et al.*, Nuclear Fusion **55**, 023002 (2015).
[16] E. Viezzer *et al.*, Nuclear Fusion **53**, 053005 (2013).
[17] R. Dux, A. G. Peeters, *et al.*, Nuclear Fusion **39**, 1509 (1999).
[18] A. G. Peeters, Physics of Plasmas **7**, 268 (2000).
[19] Q. Yu and S. Günter, Nuclear Fusion **51**, 073030 (2011).
[20] N. M. Ferraro, Physics of Plasmas **19**, 056105 (2012), http://dx.doi.org/10.1063/1.3694657.
[21] F. Orain *et al.*, Physics of Plasmas **20**, 102510 (2013), http://dx.doi.org/10.1063/1.4824820.
[22] M. F. Heyn *et al.*, Nuclear Fusion **54**, 064005 (2014).